JGR Oceans

RESEARCH ARTICLE
10.1029/2020JC016776

Long-term Observations Reveal Environmental Conditions and Food Supply Mechanisms at an Arctic Deep-Sea Sponge Ground

Ulrike Hanz[1], Emyr Martyn Roberts[2], Gerard Duineveld[1], Andrew Davies[4], Hans van Haren[1], Hans Tore Rapp[2,3,†], Gert-Jan Reichart[1,5], and Furu Mienis[1]

[1]Department of Ocean Systems, NIOZ Royal Netherlands Institute for Sea Research and Utrecht University, Texel, the Netherlands, [2]Department of Biological Sciences and K.G. Jebsen Centre for Deep-sea Research, University of Bergen, Bergen, Norway, [3]NORCE, Norwegian Research Centre, NORCE Environment, Bergen, Norway, [4]Department of Biological Science, University of Rhode Island, Kingston, RI, USA, [5]Faculty of Geosciences, Earth Sciences Department, Utrecht University, Utrecht, the Netherlands

Abstract Deep-sea sponge grounds are hotspots of benthic biomass and diversity. To date, very limited data exist on the range of environmental conditions in areas containing deep-sea sponge grounds and which factors are driving their distribution and sustenance. We investigated oceanographic conditions at a deep-sea sponge ground located on an Arctic Mid-Ocean Ridge seamount. Hydrodynamic measurements were performed along Conductivity-Temperature-Depth transects, and a lander was deployed within the sponge ground that recorded near-bottom physical properties as well as vertical fluxes of organic matter over an annual cycle. The data demonstrate that the sponge ground is found at water temperatures of −0.5°C to 1°C and is situated at the interface between two water masses at only 0.7° equatorward of the turning point latitude of semi-diurnal lunar internal tides. Internal waves supported by vertical density stratification interact with the seamount topography and produce turbulent mixing as well as resuspension of organic matter with temporarily very high current speeds up to 0.72 m s^{-1}. The vertical movement of the water column delivers food and nutrients from water layers above and below toward the sponge ground. Highest organic carbon flux was observed during the summer phytoplankton bloom period, providing fresh organic matter from the surface. The flux of fresh organic matter is unlikely to sustain the carbon demand of this ecosystem. Therefore, the availability of bacteria, nutrients, and dissolved and particulate matter, delivered by tidally forced internal wave turbulence and transport by horizontal mean flows, likely plays an important role in meeting ecosystem-level food requirements.

Plain Language Summary Sponge grounds are important ecosystems in the deep-sea that can be compared to tropical reefs. To date, very limited data exist on the range of environmental conditions in areas where deep-sea sponges and their accompanying fauna are found. In this study, we investigated environmental conditions at a deep-sea sponge ground located on the summit of an Arctic seamount. Measurements of the water around the seamount and close to the sponge ground were performed recording near-bottom physical properties as well as the food supply over an annual cycle. At the summit of the seamount, the water flow interacts with the seamount itself, which produces turbulent mixing with temporarily high current speeds. At the same time, water movements around the seamount deliver food and nutrients from water layers above and below toward the sponge ground. Fresh food from the surface water was delivered only during one major event in the summer phytoplankton bloom period. The amount of food sinking from the surface is unlikely to sustain the energetic demands of this ecosystem. Therefore, the availability of other food resources such as bacteria, dissolved and particulate matter and their delivery by water movements likely play an important role in meeting ecosystem-level food requirements.

[†]Deceased 2020.

Key Points:

- Long-term study at a deep-sea sponge ground provides environmental ranges known to support sponges
- Hydrodynamic processes deliver water with different beneficial characteristics from above and below toward the sponge ground
- Benthic organisms receive only a small amount of food sinking from the surface waters, which is likely not sustaining their energy demand

Correspondence to:
U. Hanz,
ulrike.hanz@nioz.nl

Citation:
Hanz, U., Roberts, E. M., Duineveld, G., Davies, A., van Haren, H., Rapp, H. T., et al. (2021). Long-term observations reveal environmental conditions and food supply mechanisms at an Arctic deep-sea sponge ground. *Journal of Geophysical Research: Oceans*, *126*, e2020JC016776. https://doi.org/10.1029/2020JC016776

Received 7 SEP 2020
Accepted 13 FEB 2021

1. Introduction

Benthic organisms in the deep sea largely depend on the vertical flux of organic matter from productive surface waters. Much of this vertical flux is remineralized during downward transport to the sea bottom, reducing the quantity and quality of the organic matter (Davies et al., 2009; Gooday, 2002; Kiriakoulakis

et al., 2001; Lampitt & Antia, 1997; Smetacek, 1984). Still, flourishing ecosystems, such as cold-water coral (CWC) reefs and sponge grounds, have been discovered in areas of the deep sea, where their presence cannot be explained by the amount of energy supplied by vertical flux alone (Kahn, Yahel, et al., 2015; Oevelen et al., 2009). For example, on the Canadian shelf, it was estimated that sponges consume seven times more carbon than provided by the vertical flux of organic matter (Kahn, Chu, & Leys, 2018). Therefore, additional food supply mechanisms and efficient recycling of resources must exist to fulfill this deficit.

Recently, sponge grounds have become a focus of deep-sea research since they can form hotspots of biomass and biodiversity in the deep sea similar to CWC reefs (Beazley et al., 2013; Hogg et al., 2010; Maldonado, Aguilar, Bannister, et al., 2017). At bathyal and abyssal depths sponges, specifically hexactinellids (glass sponges), belong to the most common megafaunal organisms (Tabachnick et al., 1994). Together with other sponge groups (demosponges), they are able to form extensive grounds and even reef-like habitats that cover large areas of the seafloor on shelves, slopes, seamounts, plains, and even hadal bottoms (Barthel & Gutt, 1992; Cathalot et al., 2015; Kahn, Yahel, et al., 2015; Klitgaard & Tendal, 2004; Murillo et al., 2012). Sponges are considered ecosystem engineers since they build 3D structures providing a habitat for sessile and mobile fauna, which can persist beyond their lifetime (Buhl-Mortensen et al., 2010; Meyer et al., 2019). Components of the sponge glass skeleton (so-called spicules) remain on the seafloor after their death, creating structures from several centimeters up to several meters. These spicule mats provide an important substrate for living sponges and associated fauna (Bett & Rice, 1992; Conway et al., 2005). These structures as well as the sponges themselves interact with the flow of water, leading to a modification of flow in the benthic boundary layer (BBL) which likely influences food and particle supply as well as the retention and availability of food for sponges and other suspension feeding organisms (Culwick et al., 2020; Maldonado, Aguilar, Blanco, et al., 2015; Mienis, Bouma, et al., 2019).

Sponges display a wide variety of feeding behavior that match the extreme conditions they inhabit. In addition to very specific mechanisms such as carnivory in some deep-sea sponge species (Vacelet et al., 1995), they are known to be associated with microorganisms like bacteria, viruses, and archaea which transfer food to the sponge (Hentschel et al., 2006), feed directly on bacteria from the water column (Yahel et al., 2006) or even directly take up dissolved organic carbon (DOC) as shown for tropical reef sponges (de Goeij et al., 2008; Rix et al., 2017). Therefore, they play a major role in biogeochemical cycling, for example carbon cycling, and are able to transfer organic matter from the pelagic to the benthic environment (Beazley et al., 2013; Cathalot et al., 2015).

Sponge grounds are commonly associated with increased near-bottom current velocities due to the seafloor topography interacting with local and regional hydrodynamics, similar to CWC ecosystems (Chu & Leys, 2010; Davies et al., 2009; Frederiksen et al., 1992; Rice et al., 1990). This interaction often comprises internal tidal waves enhancing currents and increasing turbulence in regions where the bed slope is comparable to the raypath slope of the internal wave propagation (e.g., Eriksen, 1982; Jalali et al., 2017; Müller & Liu, 2000; van Haren, Hanz, et al., 2017). Particularly at seamounts, but also on shelves turbulence and vertical mixing have been observed and enhanced by shear, convective instabilities from the rebounding tidal flow and breaking of transient lee waves (Davison et al., 2019; Lavelle & Mohn, 2010). Around seamounts, this has led to accumulations of pelagic as well as benthic biomass (Clark et al., 2010; Hosegood et al., 2019; Jalali et al., 2017). These processes also impact food supply from surface waters to the deep sea, increasing delivery and retention of suspended particulate matter (SPM) (Duineveld, Lavaleye, Bergman, et al., 2007). Seamounts can also induce a closed circulation above their summits (e.g., Taylor Columns), which leads to trapping of organic material or retention of resuspended organic material (Boehlert & Genin, 1987; Henrich et al., 1992; Lavelle & Mohn, 2010; G. I. Taylor, 1923).

The distribution of CWCs and sponges overlap in many areas, suggesting that similar environmental conditions are beneficial for both groups of species. However, areas consisting primarily of sponges also occur, such as for example in the NE Atlantic (e.g., Western Barents Sea, along the Norwegian Shelf to the Faroes), south of Iceland (Klitgaard & Tendal, 2004; Roberts et al., 2018), on seamounts in the Alboran Sea in the Mediterranean (Maldonado, Aguilar, Blanco, et al., 2015), the Flemish Cap, and Scotian Shelf on the Canadian shelf (Chu & Leys, 2010).

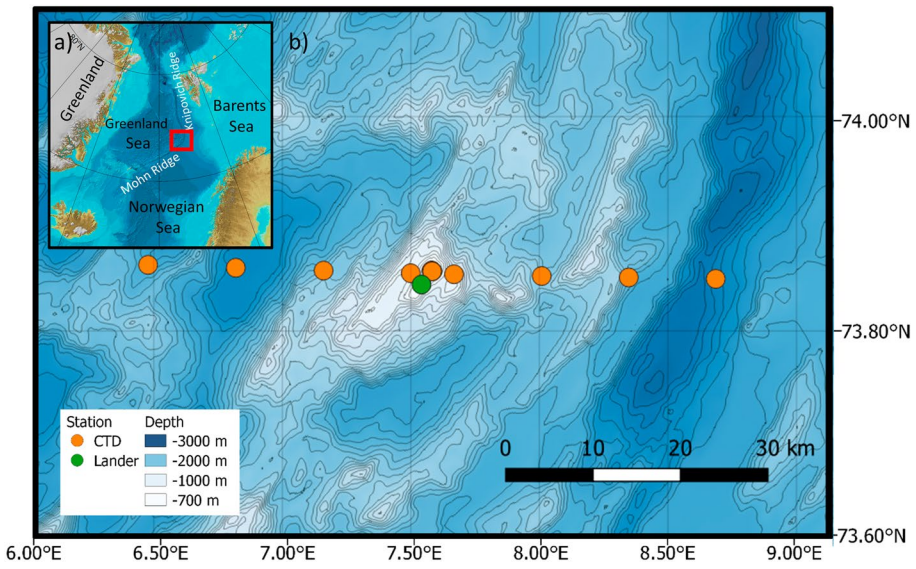

Figure 1. (a) Inset: the Schulz Bank as part of the AMOR (adapted from Jakobsson et al., 2012), (b) Map of the Schulz Bank region (contour interval 100 m) with CTD stations and position of the lander (bathymetry from Consortium, 2016). AMOR, Arctic Mid-Ocean Ridge; CTD, Conductivity-Temperature-Depth.

A recent short-term study on the environmental conditions at an Arctic seamount, the Schulz Bank, suggested that the hydrodynamic regime produces favorable conditions for the appearance of dense sponge grounds (Roberts et al., 2018). The aim of the current study was to extend these short-term observations to determine the long-term environmental drivers and their temporal variability as well as the food supply mechanisms that support the presence of a dense deep-sea sponge ground on the summit of the Schulz Bank. For this purpose, long-term near-bed observations of environmental conditions were combined with measurements of deep-sea particle fluxes. In addition, CTD profiles were recorded along transects to study the water column structure around the Schulz Bank. The ensuing data form a comprehensive set of continuous, high-resolution, long-term records of near-bed environmental conditions at a sponge ground, shedding light on the environmental ranges in which sponges are found. This study provides insight into the hydrodynamic processes that influence the sponge grounds so they can meet their energy demand in the food-limited deep sea.

2. Study Site and Methods

2.1. Regional Setting

The Schulz Bank (73° 50′ N, 7° 34′ E, Figure 1, earlier also described as the Schulz Massif seamount in Roberts et al., 2018) is part of the Arctic Mid-Ocean Ridge (AMOR). It is approximately 22 km wide and rises to about 1,900 m above the plain of the Lofoten Basin in the south and the Greenland Basin in the north. The Schulz Bank is situated between two sub-ridges, the Mohn Ridge and the Knipovich Ridge. The summit is oriented in a NE-SW direction and is situated at 600 m below the sea surface. The slope is largely dominated by soft sediments with local rocky outcrops; the summit is known to be covered by sponge spicule mats of up to 20 cm thick, overgrown by living sponges and associated fauna (Roberts et al., 2018). The highest abundance of sponges and associated fauna was found on the summit at depths above 600–800 m, below that, sponge occurrences were patchier and sponge density was significantly lower. The flanks and deeper plains showed only a sparse sponge cover. A more detailed description of sponge occurrences is presented in Roberts et al. (2018) and Meyer et al. (2019).

The water masses surrounding the Schulz Bank in the Greenland, Iceland, and Norwegian (GIN) seas have been described in detail by Hopkins (1991). The area is influenced by North Atlantic Water which is characterized by salinities >35 and temperatures >2°C (Helland-Hansen & Nansen, 1909). These waters enter from the south as a surface water mass (Norwegian Atlantic water [NwAtW]). The intermediate water mass

Table 1
Overview of Lander and CTD Stations Surveyed on the Schulz Bank From Cruises GS2016109, GS2017110, and GS2018108

Station	Device	Date	Latitude	Longitude	Depth [m]
GS2016109-07 until	Lander	21.06.2016 until	73.816	7.55234	668
GS2017110-17		27.07.2017			
GS2018108-02	CTD	31.07.2018	73.83067	7.55917	584
GS2018108-12	CTD	01.08.2018	73.82733	7.642	1,056
GS2018108-13	CTD	01.08.2018	73.82733	7.96467	2,057
GS2018108-14	CTD	01.08.2018	73.82716	8.28483	2,190
GS2018108-15	CTD	02.08.2018	73.8265	8.60483	3,000
GS2018108-22	CTD	03.08.2018	73.82983	7.56233	582
GS2018108-28	CTD	04.08.2018	73.82684	6.51617	2,479
GS2018108-29	CTD	04.08.2018	73.82733	6.839	2,972
GS2018108-30	CTD	05.08.2018	73.8275	7.162	2,111
GS2018108-31	CTD	05.08.2018	73.82733	7.48283	994
GS2018108-37	CTD	06.08.2018	73.82983	7.561	580

Abbreviations: CTD, Conductivity-Temperature-Depth.

around the Schulz Bank is Norwegian Arctic Intermediate Water (NwArIW) which originates in the GIN seas and is derived by convection from surface waters exposed to atmospheric exchange (Hopkins, 1991; Jeansson et al., 2017). Beneath this, Norwegian Sea Deep Water (NwDW) in the east and Greenland Sea Deep Water in the west are present (Rudels et al., 2002).

2.2. Data Collected in the Field

Fieldwork was conducted as part of three multi-disciplinary research cruises to the Schulz Bank (GS2016109, GS2017110, and GS2018108) with the Norwegian vessel RV *G.O. Sars* in the frame of the Horizon 2020 project SponGES. The fieldwork for the present study consisted of the deployment of a benthic lander (see below) in 2016 amidst the sponge ground for the period of one year and a CTD transect at the end of the deployment to determine water column characteristics around Schulz Bank (Table 1). During CTD casts different samples were collected from the water column (Table 1).

A CTD transect conducted in 2018 covered the deep Norwegian and Greenland basins in the east and west as well as the seamount summit to characterize the water column structure (Figure 1). The CTD profiler used was a Seabird "SBE 9 plus" underwater unit and a Seabird "SBE 11 plus V2" deck unit, equipped with a dissolved oxygen sensor (SBE 43), a chlorophyll-*a* sensor (Chelsea Aqua 3), and a rosette water sampler of 12× 10 L Niskin® water sampling bottles, triggered to close at given depths during the up-cast. For the analysis and interpretation of the measured profiles, the downcast raw data were processed with "SBE Data Processing" software.

2.3. Near-Bed Environmental Conditions

A BOBO (BOttom BOundary) lander was deployed on the summit of the Schulz Bank on the 21 July 2016 and successfully recovered on the 27. July 2017 (Figure 1, Table 1). The BOBO-lander was equipped with an Acoustic Doppler Current Profiler (ADCP; Teledyne-RDI, 1,200 kHz, recorded 13 bins of 1 m between 3.55 and 15.55 m above bottom (mab)), a combined Wetlabs turbidity and fluorometer (Wetlabs-FLNTU), a Seabird CT sensor and a combined temperature and oxygen sensor (Advantech RINKO). The ADCP sensor was attached at the top of the lander at 2 mab, all other sensors were attached around 1 mab. An HD video camera (Sony) with LED illumination was directed at the seafloor recording 30 s of video every 2 h. During the deployment all instruments were programmed at a sample interval of 15 min, except the oxygen sensor

which was set to a 30 min interval. All instruments measured during the whole deployment period, except the oxygen sensor, which stopped recording on the 01 June 2017 due to power failure. The lander was also equipped with a sediment trap (Technicap PPS4/3) with a rotating carousel of 12 bottles. The trap aperture (0.05 m^2) was at 2 mab. Sediment trap bottles were filled with a pH-buffered mercury chloride ($HgCl_2$) solution in filtered seawater collected from the deployment site and the carousel was programmed to progress in 30-day intervals. The sediment trap material was filtered over a 1 mm sieve to remove bigger particles and zooplankton. Samples were split into five sub-samples with a rotor splitter: four sub-samples were rinsed with demineralized water to remove salts and $HgCl_2$; and one sub-sample was rinsed with bottom water to keep pigments intact. All samples were freeze-dried and weighed to measure mass fluxes (Mienis, Duineveld, et al., 2012).

In this study, data of two backscatter sensors were used to identify the presence of different particle sizes. As the wavelength of sound is larger than that of light, acoustic backscatter showed the presence of larger grain sizes, about 1 mm at 1,200 kHz, while optical backscatter recorded a smaller range of particle sizes (Fugate & Friedrichs, 2002). For the time series of the acoustic backscatter signal, raw data were transferred to mean volume backscatter using the noise- and attenuation-correction of Gostiaux and Van Haren (2010). Data from bin 4 were selected, which corresponded to a height of 6.5 mab. This bin was chosen as it is close to the bottom, but high enough above the lander to minimize the effects of any flow alteration caused by the lander structure.

The near-bed horizontal velocity components obtained with the ADCP were analyzed to determine the tidal constituents contributing to currents at the Schulz Bank. The method used is an extension of the one-dimensional harmonic analysis (least squares) method commonly applied to sea-level time series data. The two velocity components were analyzed separately as a one-dimensional time series and the resulting amplitudes and phases used to define tidal current ellipses for each constituent. Top contributing constituents were assessed based on current speeds and percent energy contribution to the tidal model solution. The analyses were conducted on the horizontal velocity components averaged vertically over seven ADCP depth bins (3.5–9.5 mab) using the "UTide" package functions in MATLAB (Codiga, 2011). The length of the time series allowed a resolution of 67 constituents. Spectral analysis was performed to demonstrate the most energetic motions.

In order to assess the likelihood that the Schulz Bank sponge ground experiences intensified near-bed currents arising from incident internal tides (*sensu* Huthnance, 1989; see also Frederiksen et al., 1992), the ray slope s for an internal wave with the frequency of the dominant semi-diurnal lunar tidal constituent (M_2) was calculated according to:

$$s^2 = \frac{\left(\sigma^2 - f^2\right)}{\left(N^2 - \sigma^2\right)}$$

where f is the local inertial (Coriolis) frequency (1.4007×10^{-4} rad s^{-1} at the latitude of the Schulz Bank), N the buoyancy frequency (9.6×10^{-4} rad s^{-1}; representative value from below the permanent pycnocline) and σ the frequency of the internal tide (1.4053×10^{-4} rad s^{-1} for an internal tide with semi-diurnal lunar M_2 periodicity).

The resulting ray slope (0.68°) was compared to the bottom slopes at the Schulz Bank on the basis of multibeam data (see Figure 11, Roberts et al., 2018).

Vertical water displacement was estimated by comparing the CTD profile with the lander time series. The recorded temperature change during one day (ΔT; determined from maximum and minimum temperatures) measured by the lander was compared with the corresponding temperatures and depths in the CTD transect during the same time interval.

2.4. Suspended Particulate Matter: C/N Analysis, Isotope, and Chlorophyll Measurements

Sediment trap material was transferred into silver cups and the material was acidified inside the cups (2 M HCl). $\delta^{15}N$ ($^{15}N/^{14}N = \delta^{15}N$), $\delta^{13}C$ ($^{13}C/^{12}C = \delta^{13}C$) and total weight percent of organic carbon and nitrogen

were analyzed on an Elemental Analyzer (EA; Flash 2000) coupled via an open split (Conflo IV, Thermo Fisher Scientific Inc.) to an Isotope Ratio Mass Spectrometer (IRMS; Thermoscientific, Delta V Advantage). For nitrogen stable isotope analyses pure N_2 was used as a reference gas. As a standard for $\delta^{13}C$ benzoic acid and acetanilide was used, while for $\delta^{15}N$ acetanilide, urea and casein were used. Values are reported in per mille relative to air (N_2) and VPDB (C) respectively. For $\delta^{13}C$ analysis a high signal method was exercised including a 70% dilution. Precision and accuracy based on replicate analyses and comparison of standards to their certified values was better than 0.15 ‰ for both $\delta^{13}C$ and $\delta^{15}N$. Chlorophyll-*a* was extracted from sediment trap samples by adding 90% acetone under dark and cool conditions (Wakeham et al., 1993). The concentration was measured by a Fluorescence Spectrometer (F-2500 FL Hitachi) by comparing the sample absorbance to the absorbance of a known chlorophyll-*a* standard at two wavelengths (431.0 and 671.0 nm). Afterward HCl was added to the sample to break down chlorophyll-*a* and measure degradation products (pheophytin-*a*). The amount of chlorophyll-a compared to degradation products was then calculated (for details see Holm-Hansen et al., 1965).

3. Results

3.1. Water Column Data

At the surface, NwAtW was observed and reached depths deeper than 700 m in the basin east of Schulz Bank while the thickness of the NwAtW gradually decreased in extent toward the west (Figure 2). East of the summit of Schulz Bank NwArIW is constrained at a depth of 1,000–1,500 m which is in contrast with the western side where it is also located shallower. NwArIW has a density anomaly between 27.70 and 27.97 kg m^{-3} (Rudels et al., 2002, Figure 2a). NwArIW features a local dissolved oxygen (DO) concentration maximum between 500 to 1,000 m water depth (Figure 2e). Below about 1,000 m and at a density anomaly >28.05 kg m^{-3} NwDW ($T < -0.5$°C, salinity of 34.91–34.92) was observed. In 2018, the summit of the seamount was somewhat above the interface between NwArIW and NwDW, where it was observed in 2016 (Roberts et al., 2018). As NwArIW contained more oxygen than NwDW, the oxygen data provide good insight into the characteristics of the interface between the two water masses. Fluorescence maxima were observed at approximately 50 m water depth, declining to <0.1 μg l^{-1} below (data not shown) as was also observed by Roberts et al. (2018).

The square of the buoyancy frequency, N^2, is a measure of stratification stability, and was calculated from the density profile at a CTD station on the eastern side of the Schulz Bank. In this case, two maxima in N^2 were observed (Figure 3). A strong stratification was found underneath the surface mixed layer at about 50 m and a second, weaker pycnocline was identified at a depth of 500 m ($N^2 = 0.00001$ s^{-2}, Figure 3b). The deeper pycnocline was situated at the interface between NwAtW and NwArIW. No N^2 peak was situated at the interface of intermediate and deeper water masses.

The height of internal waves was estimated by comparing temporal and spatial measurements of temperature (see Section 2). In July 2017, the maximum isopycnal displacement was calculated to be around 210 m (−0.2°C to 0.1°C temperature fluctuations during one day corresponds to 870 and 660 m depth in the water column, respectively).

3.2. Lander Data

3.2.1. Setting

Visual information recorded by the camera on the BOBO-lander confirmed that the lander was deployed within an area densely covered with sponges and associated fauna, including anemones, soft corals, tunicates (Figure 4) as well as mobile fauna like sea urchins, brittle stars, starfish, and grenadier fish, which appeared temporarily in some videos. Analysis of the video clips taken by the lander demonstrated that there were no major changes in benthic cover, size of the organisms and species abundance during the deployment. Several events with strong currents were observed, whereby some benthic organisms were affected. For example, anemones and soft corals retracted their tentacles and some anemones, tunicates and larger sponges (likely *Schaudinnia rosea*) were observed to be relocated by the currents (Hanz, 2019).

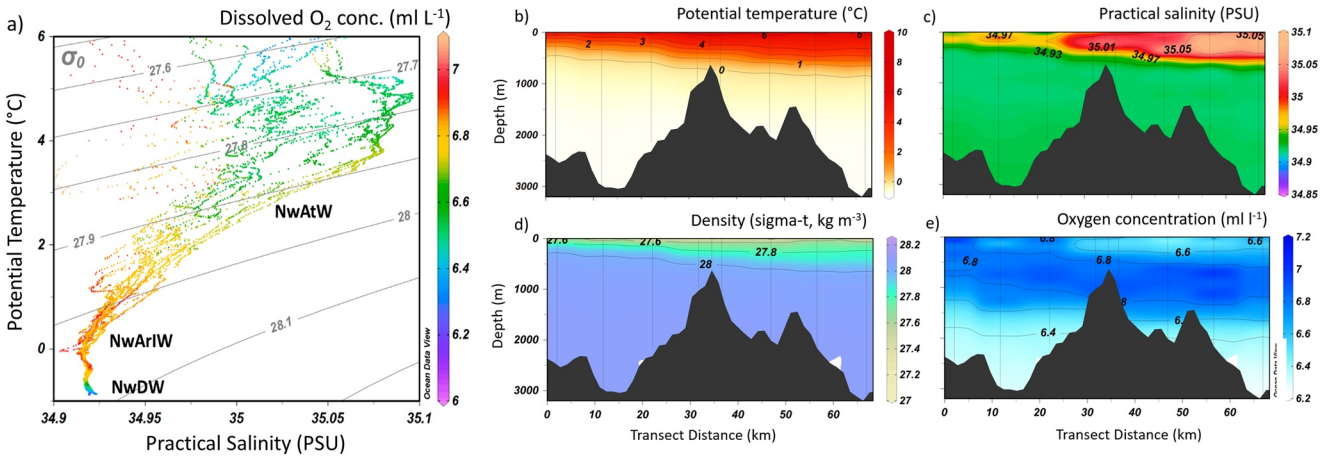

Figure 2. (a) TS diagram including isobars and water masses indicated. CTD transect cross-sections of (b) potential temperature, (c) salinity, (d) density anomaly (sigma-t), (e) DO concentration in August 2018. Vertical lines indicate CTD locations (data plotted using Ocean Data View v.4.7.8; Schlitzer, 2015). CTD, Conductivity-Temperature-Depth; DO, dissolved oxygen.

3.2.2. Long-term Records

The most striking observation of the long-term record was that near-bed water temperatures were low throughout the year, varying around a mean of 0°C (−0.5°C to 1°C, Figure 5a). The highest temperatures were observed in November–December, while lowest temperatures were recorded in March, April and August (min. of −0.5°C). Spring and neap tidal cycles were observed in the temperature record from March to August. From September to December temperature increased toward a maximum of 1°C. In December, short-term temperature fluctuations were largest and sometimes were as large as 1°C during one day, which coincided with high current speed. DO concentrations decreased from October to January until they increased in January (Figure 5b). After late March, periodical fluctuations of DO concentrations were recorded. The oxygen concentration was varying between 8.4 and 9.1 ml l^{-1}. Fluorescence was in general low and showed only one major peak at the end of May (Figure 5c). Turbidity (based on acoustic backscatter measurements) increased from September to October and also during a short period in December (Figure 5e). In December, higher turbidity was corresponding to periods of high current speed.

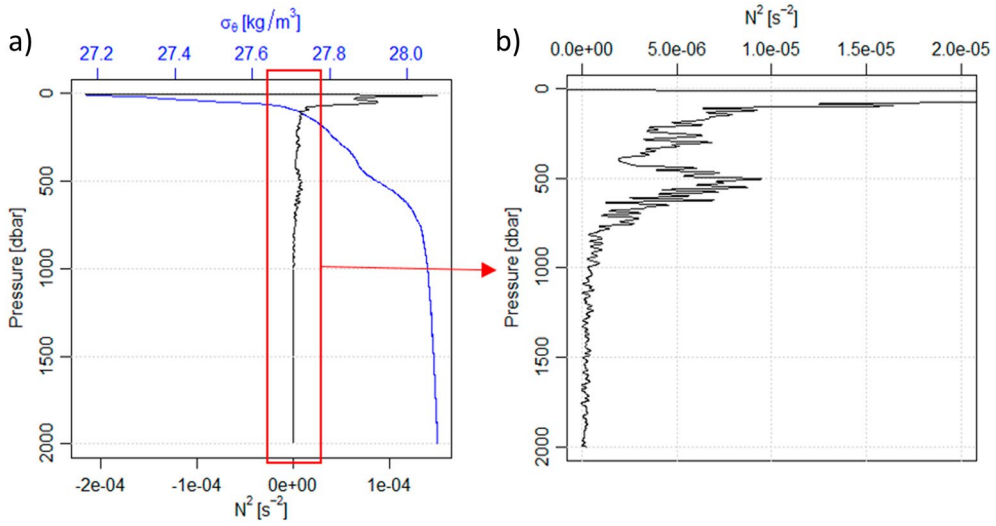

Figure 3. (a) Buoyancy frequency N^2 (black) and density (blue) of CTD station slightly east of the seamount, (b) zoomed-in view of the second peak around 500 dbar. CTD, Conductivity-Temperature-Depth.

Figure 4. Camera view from the lander showing sponges as well as associated fauna, including anemones, soft corals, tunicates on top of a dense spicule mat. (a) Video still captured at the start of the deployment 04 June 2016, (b) Video still captured at the end of the deployment at 15 July 2017.

The acoustic backscatter recorded constantly elevated values in the BBL up to about 6 mab (Figures 5e and 6). This turbid layer was thinner from April to June (up to 4 mab) and thicker during resuspension events in autumn and winter (over 10 mab, Figure 6). Periods of high turbidity in the BBL were connected to slow southwestward currents in the first 5 mab (<0.07 m s^{-1}). Water flow at the summit of the seamount exhibited an asymmetry in the tidal transport, with net residual transport in the WNW (290°) direction over the summit (Figure 7). Current speed at a depth of 6.5 mab showed daily fluctuations of about 0.4 m s^{-1} around an average of 0.14 m s^{-1}, whereas highest current speeds of up to 0.76 m s^{-1} were recorded in December (Figure 5f). Slowest current speeds were related to a southward directed flow.

The optical backscatter sensor at 1 mab recorded only one major turbidity peak in December (Figure 5d) and a smaller peak after the peak in fluorescence in May 2017, indicating an increase of smaller particles in the SPM fraction, while mostly larger particles predominate at the end of summer/autumn as shown by the acoustic backscatter record. This was confirmed by comparing the video observations for the different

Figure 5. Time series of (a) temperature, (b) oxygen concentration, (c) fluorescence, (d) optical and (e) acoustic backscatter and (f) current speed with 0.3 cycles per day cut-off low-pass filtered current speed, measured by the lander on the summit of the Schulz Bank from July 2016 to August 2017.

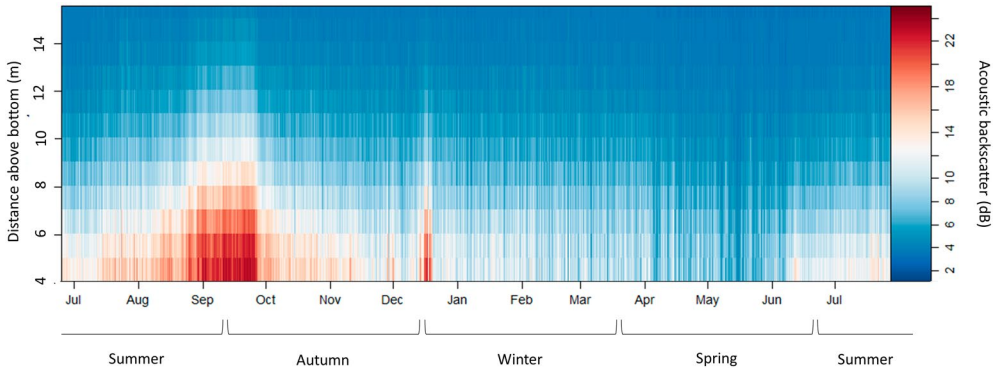

Figure 6. Acoustic backscatter intensity at 4–15 m above bottom during the period July 2016 until August 2017.

time intervals, with large, slow moving marine snow being observed at the end of summer and fast moving particle aggregates and sponge spicules being observed in winter, specifically during the high current speed events.

3.2.3. Tidal Analysis

The primary astronomical constituents determined for the observed current signal were the principal lunar semi-diurnal (M_2) constituent, contributing about 38% energy to the tidal model solution, and the luni-solar declinational diurnal (K_1) constituent, contributing 24% energy. This is evident in the kinetic energy spectrum, in which the largest peaks were found at these frequencies (Figure 8). The local inertial frequency is very close to M_2 and does not show a separate distinguishable peak. In terms of internal waves, $K_1 < f$ and thus waves are non-propagating or trapped, while $f \leq M_2 \leq N$ permits freely propagating waves with the notion that M_2-waves propagate near-horizontally.

The M_2 satellite constituents H_1 and H_2 (with frequencies very close to that of M_2) were indicating seasonal modulation of the amplitude and phase of the M_2 harmonic. Some variations on seasonal timescales captured by the fitting procedure (including the M_2 modulation and solar semi-annual constituent) may be the result of non-tidal processes (e.g., seasonal changes in stratification and associated changes in tidal currents through internal tides). The compound tide MKS_2 contributes 6.7% energy to the tidal model solution, and thus the nonlinear interaction of astronomical tides that this harmonic represents is relatively important.

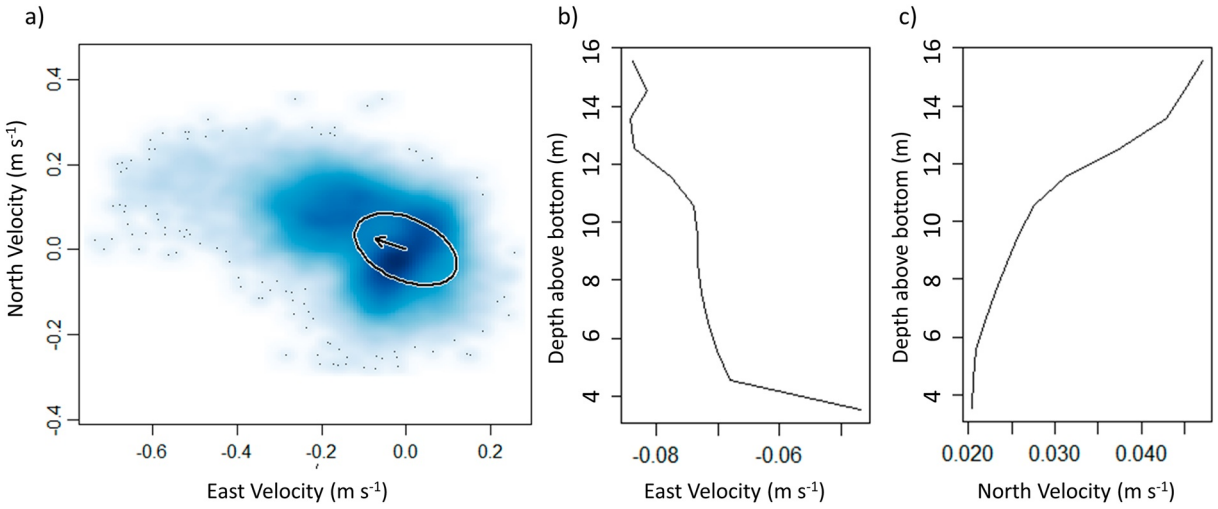

Figure 7. (a) Time-averaged flow velocity in the horizontal at the Schulz Bank summit during one year with the tidal ellipse and residual current indicated by an arrow, (b) Time-averaged eastward flow velocity per depth above the bottom during one year, (c) Time-averaged northward flow velocity per depth above the bottom.

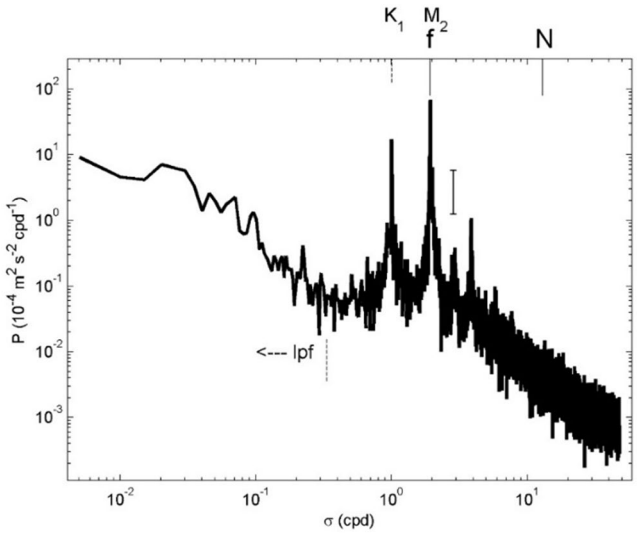

Figure 8. Weakly smoothed, about 10 degrees of freedom, average kinetic energy spectrum from currents of bins 2–4, with indications at tidal frequencies diurnal K_1 and semi-diurnal M_2, inertial frequency *f*, and buoyancy frequency *N*. The lower vertical dashed line indicates the cut-off frequency for low-pass filtering.

The superposition of all 67 constituents in the fit explained 44.3% of the observed variance in the original currents record (i.e., 44.3% tidal variance, *sensu* Codiga, 2011). The mean current components were found to be 0.022 m s^{-1} and −0.067 m s^{-1} for the north and east components, respectively, confirming a mean current of 0.071 m s^{-1} flowing west-northwest (288.2°).

The residual or "de-tided" signal in the horizontal velocity data was computed by subtracting the reconstructed tidal signal (based on the amplitudes and phase lags determined by harmonic analysis) from the original record. It revealed that high current events, particularly those in December, were not well captured by the tidal model (i.e., they remained strongly present in the residual component of the time series and were thus non-tidal in nature)—see the tidally low-pass filtered record in Figure 5f. Sub-tidal flows are dominated by a small peak at 0.2 cpd (cycles per day), implying a 5 day periodicity. Larger broadband "peaks" are found at 0.02 cpd (50-day periodicity) and 0.005 cpd (200-day periodicity), see Figure 8. The direction of the large-scale sub-tidal flows is mainly east-west (cf. Figure 7a), or about a 45° angle with the main ridge of Schulz Bank.

Intensified near-bed currents, caused by internal tides being amplified by the topography, are generated most effectively where the bottom slope is equal to or larger than the ray slope of the internal wave. These intensified currents were calculated to appear in areas where the slope of the Schulz Bank exceeds 0.68°, for the dominant M_2 constituent (for calculation see Section 2).

At the lander site, bottom slopes are about 7° and are thus supercritical for M_2 propagating internal waves. The site of Schulz Bank is very close to the turning point latitude for M_2 internal tidal waves, which become evanescent poleward of 74.5°N and thus reflect equatorward. At the turning point latitude, which is only 0.7° poleward of the lander site, internal wave energy is expected to be enhanced (e.g., Munk, 1980) and internal tides propagate near-horizontally like inertial waves.

3.2.4. Short-term Fluctuations

In order to determine relationships between physical factors and the resuspension of suspended material, two shorter periods of two days were analyzed. Two days in December with large semi-diurnal current fluctuations were compared with two days in July with small diurnal current fluctuations, being essentially the extremes from the entire observation period.

In winter current speeds varied in a semi-diurnal pattern from 0.2 m s^{-1} to 0.7 m s^{-1}. Low current speed was correlated with a southward current direction, high currents with a northwest current direction. Peaks in the acoustic backscatter did not appear to be strictly associated with one part of the tidal cycle. Sometimes turbidity peaks appeared during slow southward current, whereas other turbidity peaks were in line with peaks in current speed (Figure 9). In contrast to semi-diurnal tides in winter, during summer a predominantly diurnal current pattern was observed with much smaller semi-diurnal constituents and current maxima less than half those observed for the winter season (Figure 9a). Highest currents in summer, as with winter, were in a northwest direction and slower currents in a southern direction. Acoustic backscatter did not correlate with the current speed in summer.

3.2.5. Vertical Fluxes

Vertical downward mass fluxes showed three peaks in September 2016, December 2016, and June 2017 all exceeding 200 mg dry matter m^{-2} day^{-1}, while during spring and early summer mass fluxes were below 100 mg m^{-2} day^{-1} (Figure 10a). The carbon flux peaked in June 2017, when it exceeded 20 mg C_{org} m^{-2} day^{-1}. Comparing mass and carbon fluxes showed that the 2016 September and December peaks in mass flux were relatively low in organic carbon, indicating resuspension of material as was shown by high backscatter values, high current speeds and in the video footage. This was confirmed by the presence of large amounts

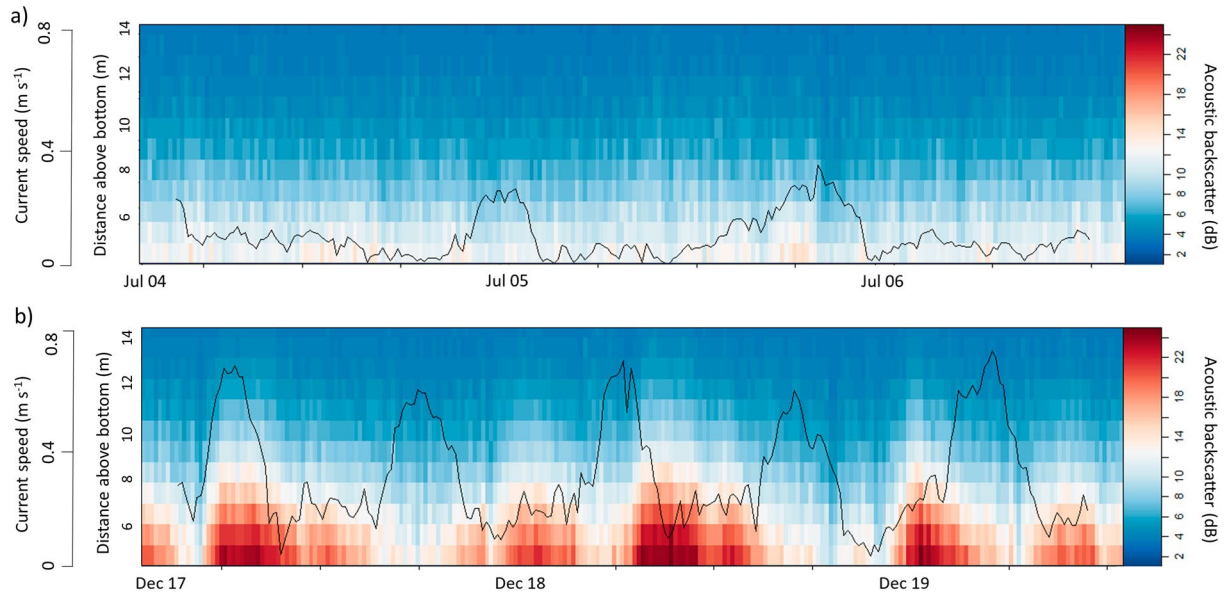

Figure 9. Acoustic backscatter from 4 to 14 mab and current speed at 6.5 m above seafloor (black line) at two days (a) in summer, (b) in winter.

of sponge spicules in the collected trap material for these periods. The $\delta^{15}N$ of the sediment trap material increased from 2.2‰ in July 2016 to 7.5‰ in June 2017 (Figure 10b). The $\delta^{13}C$ value was on average −24.88 ‰ (data not shown). Over the same time interval the C/N ratio decreased from 7.4 to 5.2 (Figure 10a). The chlorophyll-*a* concentration decreased from about 50 μg l^{-1} in July 2016 to 0 μg l^{-1} in November 2016 and

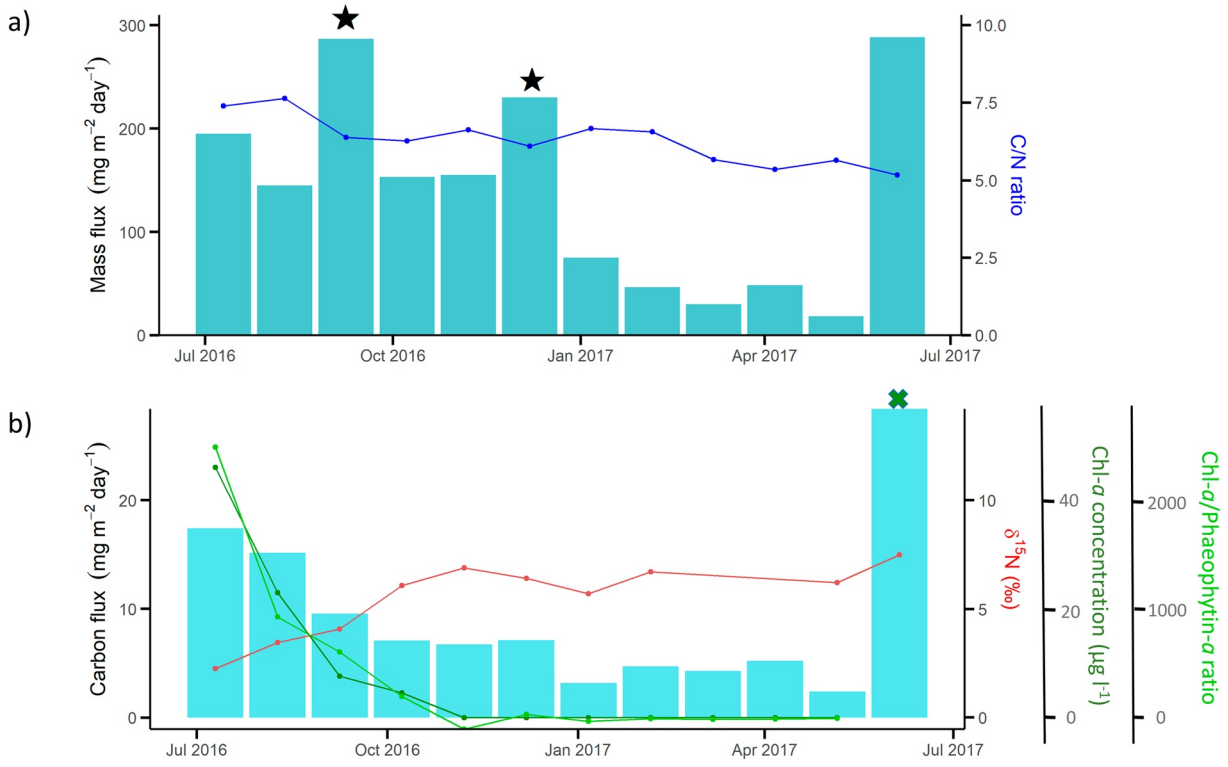

Figure 10. (a) Vertical mass flux at the sponge ground and C/N ratio (b) Carbon flux, $\delta^{15}N$, chlorophyll-a concentration and chlorophyll-a/pheophytin-a ratio of the sediment trap material from July 2016 to July 2017 in 30 day intervals. Stars indicate resuspension events; green cross indicates missing chlorophyll-a value.

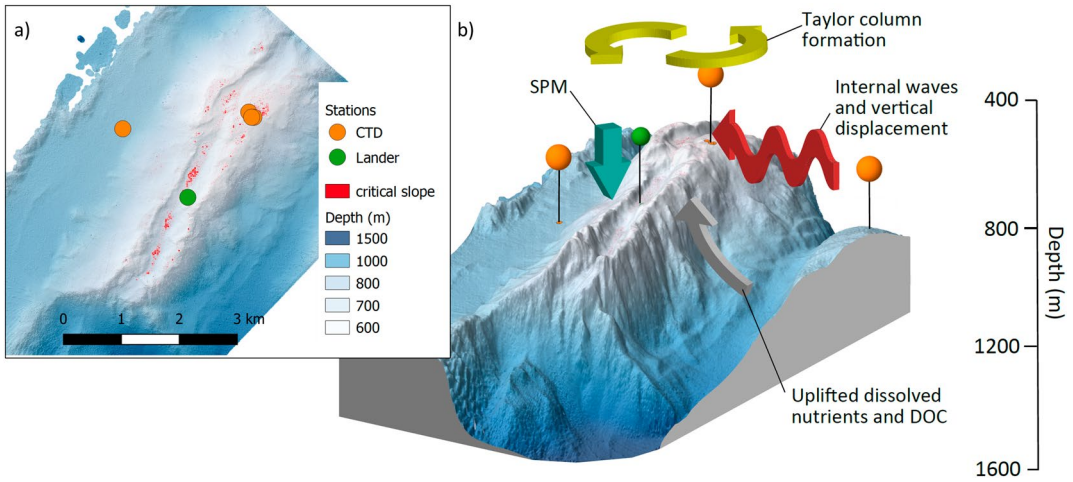

Figure 11. (a) Summit of the Schulz Bank from multibeam echosounder data (5 m resolution) with critical slope areas for semi-diurnal internal waves marked in red. The slopes were calculated over a 5X larger neighborhood of cells to better visualize areas of critical slope, (b) 3D representation of the Schulz Bank summit with dominant hydrodynamic features and food supply mechanisms indicated. DOC, dissolved organic carbon.

stayed at 0 $\mu g\ l^{-1}$ until June 2017 (no value for July 2017, Figure 10b). The chlorophyll-*a*/pheophytin-*a* ratio was highest in July 2016 (2,488) and decreased during the sampled time interval.

4. Discussion

Deep-sea sponge grounds are hotspots of biological activity, yet their environmental requirements, in terms of hydrodynamics and food supply mechanisms are so far poorly known. This study shows the first observations of the long-term near-bed environmental conditions at a sponge ground in the Arctic. It provides insight into the variability of physical and biological conditions deep-sea sponges are experiencing throughout a year.

4.1. Temperature

Bottom water temperatures on the Schulz Bank summit were around 0°C during the whole 13 months of observations, which might have important implications for the benthic communities. In general, low temperatures slow chemical reactions and reduce enzyme activities (Hochachka & Somero, 1968). This has a major effect on the functioning of (benthic) organisms as it controls metabolic rate and physiological processes slow down with decreasing temperature (King & Farner, 1961; Strand et al., 2017). A slower metabolism reduces energy demand in most aquatic invertebrates, where respiration rates are roughly halved with every 10°C decrease (Q_{10} temperature coefficient = 2–3, e.g., Coma, 2002). It is known that benthic species can adapt to cold environments, which compromises extrapolation of the metabolic rates of tropical or temperate species down to cold environments (Somero, 1998). Still, the cold environment might play a role in the survival of species in this food-deprived environment due to reduced metabolism, whereas food reduction itself might also decrease the metabolic state like for example observed in fish (Yang & Somero, 1993). The upper temperature range for deep-sea sponge occurrences is not known for most species, whereas for example *Geodia barretti* (characteristic for boreal grounds) is known to survive in temperatures of up to 12°C (Strand et al., 2017). Our long-term record showed that deep-sea sponges in Arctic grounds thrive at temperatures at least 4°C lower than the reported temperature range of, for instance, scleractinian CWCs (4°C–12°C, Dodds et al., 2007; Freiwald, 2002). *Pheronema carpenteri*, a relatively well-known glass sponge, has been found over a broad temperature range of 2.7°C–20.9°C (Howell et al., 2016). These thresholds imply that sponges could be more prevalent in the deep sea compared with CWSs.

4.2. Hydrodynamics

Density gradients play an important role in mixing processes in the ocean interior. In general, less mixing is found in a highly stratified water column. Nevertheless, baroclinic tidal waves are able to propagate along density gradients inside the ocean interior. The ability of internal waves to propagate freely depends on the turning point latitudes. At the latitude of the Schulz Bank, they can only exist at a semi-diurnal frequency since diurnal internal tides cannot exist as freely propagating waves at this latitude (Lavelle & Mohn, 2010; Robertson et al., 2017). However, around Rockall Bank trapped diurnal tidal waves have been demonstrated to considerably contribute to turbulent mixing over coral mounds (Cyr et al., 2016; van Haren, Mienis, et al., 2014). The large diurnal tidal signal observed in our data suggests a similar mechanism is at work around Schulz Bank. In addition, the latitude of Schulz Bank is so close to the turning point latitude of M_2 internal tides that enhancement of internal tidal energy is expected (Munk, 1980).

If propagating internal tidal waves impinge on topographic features like seamounts, they can be reflected or their energy can be converted into turbulence depending on the properties of the obstacle (Jalali et al., 2017). Turbulence is created by internal waves propagating upslope and interacting with the downslope flow, which remains from previous waves, resulting in wave breaking (J. R. Taylor, 1993). This can produce high local turbulence around the seamount summit (van Haren, Hanz, et al., 2017). At the Schulz Bank, we observed strong semi-diurnal and diurnal tides which are likely the origin for high internal wave breaking, increasing local mixing and turbulence. Intensification and amplification of both turbulence and mixing at the Schulz Bank is expected to appear in areas where the bed slope is steeper than that of semi-diurnal internal tidal wave slopes of around 0.68° (Figure 11). Unfortunately, there was not enough fauna distribution data available to correlate the steeper slopes of the summit with an increased abundance of benthic organisms. However, it is known that steep slopes on the north-eastern summit are an area of high species abundance (Meyer et al., 2019).

We established the characteristics of the internal waves at Schulz Bank by comparing temporal and spatial measurements (see Section 2): isopycnal displacements are up to >200 m and peak near-bed horizontal current velocities are up to 0.7 m s^{-1}. These velocities are much higher than found at other biologically rich Mid-Atlantic seamounts (van Haren, Hanz, et al., 2017; van Haren & Gostiaux, 2012) and are comparable to currents associated with internal waves at the Hawaiian ridge, which were observed to be up to 300 m in displacement (Rudnick et al., 2003), or over a CWC mound at the Rockall bank, which were more than 120 m high (van Haren, Mienis, et al., 2014). The maximum current speeds at Schulz Bank were close to those of internal waves observed in the South China Sea, where horizontal velocities of up to 1 m s^{-1} were found producing massive overturns of up to 500 m, which are expected to be amongst the most powerful in the world (Alford et al., 2015). Resulting turbulence in such regions can be >1,000 times that of the open ocean (van Haren & Gostiaux, 2012), which is also suggested to be beneficial for CWCs (Mienis, Duineveld, et al., 2012). Video recordings taken during highest current speed events in winter at Schulz Bank showed that these might be close to the maximum that sessile benthic fauna can endure, with some individual sponges as well as anemones already being detached from the bottom and transported laterally (Hanz, 2019).

Mixing processes due to turbulence and the vertical displacement of water with different properties are likely to be an essential driver for the local benthic fauna since they supply nutrients, oxygen, and particulate organic matter (Duineveld, Lavaleye, & Berghuis, 2004). Comparison of the baroclinic tides with SPM supply to the sponge ground in this study indicated that tidal waves might provide an alternative route for delivering nutrients from deeper water layers and possibly even fresher SPM from shallower water masses as a consequence of enhanced downward currents on short-time scales as was also observed near CWCs (Duineveld, Lavaleye, Bergman, et al., 2007). Once brought into suspension by turbulent mixing, the suspended matter will be advected horizontally by the larger-scale flows. These flows are, on average, directed approximately westward over Schulz Bank. Since we did not study potential sources further away from Schulz Bank, we have no quantitative measure of the supply of organic matter to the Schulz Bank from the east. Mixing around the seamount is likely to deliver water column bacteria toward the sponge communities on the summit, which act as a food source. This process has been observed to influence the microbial community structure up to several hundreds of meters above the summit (Busch et al., 2020).

Hydrodynamic processes can also trap food particles above the seamount summit. Earlier modeling studies (Chapman & Haidvogel, 1992) showed that anti-cyclonic circulation patterns (*Taylor caps)* or *trapped waves* in the case of periodically alternating flow can arise over the summit of isolated seamounts (Haidvogel et al., 1993). These have the potential to trap sinking organic material (Mourino et al., 2001; Vilas et al., 2009), but can also affect the microbial community composition (Busch et al., 2020). Roberts et al. (2018) expected possible transient Taylor caps at the Schulz Bank. Calculations in this study with an updated larger dimension of the seamount ($h = 1.9$ km, $L = 22$ km, $H = 2{,}460$ m, $U = 0.14$ m s^{-1}) confirms the possibility of a Taylor cap ($R_o = 0.045$, $\delta = 0.77$, $S = 2.55$, $f = 1.4 \times 10^{-14}$ rad s^{-1}, $N = 3.2 \times 10^{-13}$ s^{-1}, calculations like stated in Roberts et al., 2018). However, evidence for a Taylor cap in the form of clear isopycnal doming, higher turbidity or increased fluorescence above the summit, as shown in Roberts et al. (2018), were not detected by the CTD transect in 2018. This likely reflects the coarse spatial resolution of the CTD transect or the timing of the CTD transect not corresponding with the main bloom period or with a Taylor cap that is transient in nature.

4.3. The Reef Effect

Benthic food availability also depends on smaller-scale processes entraining food resources in the BBL (Boudreau & Jorgensen, 2001). Particulate matter was continuously resuspended above the sponge ground as indicated by a turbid BBL throughout the year. Short-term observations showed that this BBL experiences periods where the extent of the turbidity in the BBL decreases. These periods are likely essential to replenish the BBL with new suspended (organic) matter as well as dissolved (organic) matter, bacteria (Busch et al., 2020), and nutrients, which all serve as a food source for the benthic fauna. Roberts et al. (2018) showed that water in the BBL is also replenished by water with higher DO concentration during so-called jump-relax events.

In the 5 m immediately above the bottom, currents interact with the "roughness" of the bottom created by the 3D structure of the benthic fauna and sponges (Witte et al., 1997), which creates additional small-scale turbulence, as observed at CWC reefs (Guihen et al., 2013; Mienis, Bouma, et al., 2019). This turbulence may play a role in the trapping and accumulation of particles in the lower BBL. Significant differences between the current speeds below and above 5 mab (Figure 6) as well as in the long-term permanent turbid layer from 2 to 6 mab in the acoustic backscatter record (Figure 5) are indicating the presence of this reef effect at the Schulz Bank sponge ground.

4.4. Fluxes of Organic Matter

One peak in fluorescence was observed at the end of May at the Schulz Bank summit corresponding with a high flux of organic matter. The presence of only one bloom period is typical for the Arctic region (Sverdrup, 1953). At high latitudes, the spring bloom occurs late without a subsequent fall bloom, depending on the onset of the stabilization of the upper water layer and the limited sun elevation (Wassmann et al., 1991). The Arctic summer phytoplankton bloom at the surface delivered OM of relatively high nutritional quality to the Schulz Bank sponge ground in July 2017 and especially June 2016, when $\delta^{15}N$ reached its lowest value and chlorophyll-*a* values were highest, indicating the presence of relatively fresh phytodetritus at the sponge ground (Figure 10). However, the C_{org} flux throughout the year was in general low during all other months. After the 2016 bloom period the C_{org} flux decreased to reach a minimum just prior to the onset of the next bloom period in June 2017. The June 2017 peak in vertical flux in our sediment trap does not seem to be composed of sinking fresh primary production because of the relatively high $\delta^{15}N$. More likely the material is derived from fecal pellets of copepods (*Calanus* sp.) which contain degraded phytodetritus (Nöthig & von Bodungen, 1989). According to Bathmann et al. (1990) copepod abundance decreases significantly after the fecal pellet pulse in June/July due to insufficient food resources and small quantities of unprocessed organic material can sink to the bottom. This would explain the relatively fresh organic matter in our sediment trap in months following the July 2016 peak in C_{org} flux (Figure 10). In September light intensity in the Arctic is insufficient for substantial primary production, inhibiting a second bloom and therefore there is no further delivery of fresh material to the sponge ground. After the summer period more processed (i.e., refractory) organic material was observed in the sediment trap, based on increasing $\delta^{15}N$ values and decreasing chlorophyll-*a* content, which is most likely derived from resuspended or advected

sediments. Resuspension events were observed in our data when turbidity increased in the BBL from that time onwards (Figure 6). High turbidity events in winter are produced by resuspension of material from the bottom, which is confirmed by the fact that a large amount of spicules and a low carbon content was found in the sediment trap at these times. The combined data suggest that the benthic community on Schulz Bank depends on the food pulse of fresh material in summer refueling the BBL with high-quality SPM, which becomes progressively more refractory and depleted over the remainder of the year.

The food delivered to the sponge ground has likely no allochthonous source since no landmasses are close enough to deliver terrestrial organic material. Terrestrially derived organic material has a higher C/N ratio (>10) and generally shows a depleted $\delta^{13}C$ signal around −27‰ (Knies & Martinez, 2009), compared to the values recorded here, which were showing a marine origin (C/N <10 and $\delta^{13}C$ of <26 ‰).

There are so far no data available on community carbon uptake by the sponge ground on Schulz Bank to match with the C flux measured here. Taking the estimated carbon demand of a deep-water glass sponge reef (ca. 160 m depth, ~10°C) at the Canadian coast (1,800–4,100 mg C m^{-2} day^{-1}, Kahn, Yahel, et al., 2015), the carbon input at Schulz Bank during the bloom period with the highest carbon input would provide approximately <1% of the required carbon demand. In the Canadian sponge reefs C consumption was much higher compared to the carbon flux (460 mg m^{-2} day^{-1}). However, this estimation does not include the potential changes or adaptations in metabolism depending on depth and temperature. Even though it is difficult to compare both ecosystems, it is likely that the low carbon flux will at no time cover the carbon demand of the densely covered sponge ground of the Schulz Bank even if the actual demand is much lower than that in sponge grounds of the Canadian coast. This is based on sediment trap data which presumably underestimates the vertical flux (Baker et al., 1988), which implies that the assumed carbon deficit is slightly smaller. Therefore, it is to be expected that the availability of dissolved organic matter (de Goeij et al., 2008), pelagic bacteria (Reiswig, 1975; Yahel et al., 2006) and chemosynthesis by symbiotic bacteria and archaea (Hentschel et al., 2006; Radax, Hoffmann, et al., 2012) will play an important and supplementary role in meeting the food supply demands of the Schulz Bank sponge community (Busch et al., 2020). To enhance these processes, the hydrodynamic regime will play an important role. Internal wave actions will transport water from deeper areas with higher dissolved nutrient concentrations (PO_4, NO_x, Si) toward the summit with each tidal cycle (Roberts et al., 2018). This is detectable by the temperature records measuring water from deeper or shallower regions with a difference of up to 1°C and the calculated vertical displacement of >200 m water depth. This can fuel the bacterial and Archean communities at the sponge ground, as well as the sponges and their own bacterial communities directly (Busch et al., 2020; de Goeij et al., 2008; Radax, Rattei, et al., 2012). Turbulence at the seamount summit due to interaction of internal waves with the seamount topography is proposed as the essential factor allowing a constant replenishment of both resources (resuspended SPM and inorganic nutrients) in the BBL, resulting in a dense coverage of filter-feeding and microbially active sponges.

5. Conclusion

The 1-year data set on near-bed environmental conditions showed that sponges can withstand temporarily high current speeds (~0.7 m s^{-1}), live in temperatures around 0°C and can survive in an environment which likely does not receive sufficient food from surface waters to be able to sustain such a dense benthic ecosystem. Although we do not have quantitative evidence of the suspended matter and nutrient sources, larger-scale flows may have transported these from the east and greater depths. A major finding was that the sponge ground is located at the interface between two water masses, where strong internal tidal waves can propagate and interact with the bottom topography. Being near the M_2-turning point latitude, enhanced semi-diurnal (as well as trapped diurnal) internal tides slosh back and forth against the steep slopes causing wave breaking. This creates mixing and turbulence on the seamount summit, delivering and exchanging water with different beneficial characteristics from above and below, thereby supplying the benthic ecosystem with new resources (e.g., particulate and dissolved matter) within a semi-diurnal tidal cycle.

Conflict of Interest

The authors declare no conflicts of interest relevant to this study.

Data Availability Statement

Lander and CTD data are available in PANGAEA (Hanz, 2021a, 2021b, 2021c). The lander video data are available in the NIOZ data repository (Hanz et al., 2019). CTD data: https://doi.org/10.1594/PANGAEA.927946. Sediment trap: https://doi.org/10.1594/PANGAEA.927955. Long-term: https://doi.org/10.1594/PANGAEA.927956. Video: https://doi.org/10.25850/nioz/7b.b.t

Acknowledgments
This research has been performed in the scope of the SponGES project, which received funding from the European Union's Horizon 2020 research and innovation program under grant agreement No. 679849. This document reflects only the authors' views and the Executive Agency for Small Medium-sized Enterprises (EASME) is not responsible for any use that may be made of the information it contains. Daniel Codiga is thanked for his advice on applying the MATLAB package UTide. Furu Mienis is supported by the Innovational Research Incentives Scheme of the Netherlands Organisation for Scientific Research (NWO-VIDI grant no. 0.16.161.360).

References

Alford, M. H., Peacock, T., MacKinnon, J. A., Nash, J. D., Buijsman, M. C., Centurioni, L. R., et al. (2015). The formation and fate of internal waves in the South China Sea. *Nature*, *521*(7550), 65–69.

Baker, E. T., Milburn, H. B., & Tennant, D. A. (1988). Field assessment of sediment trap efficiency under varying flow conditions. *Journal of Marine Research*, *46*(3), 573–592.

Barthel, D., & Gutt, J. (1992). Sponge associations in the eastern Weddell Sea. *Antarctic Science*, *4*(2), 137–150.

Bathmann, U. V., Peinert, R., Noji, T. T., & Bodungen, B. V. (1990). Pelagic origin and fate of sedimenting particles in the Norwegian Sea. *Progress in Oceanography*, *24*(1–4), 117–125.

Beazley, L. I., Kenchington, E. L., Murillo, F. J., & Sacau, M. d. M. (2013). Deep-sea sponge grounds enhance diversity and abundance of epibenthic megafauna in the Northwest Atlantic. *ICES Journal of Marine Science*, *70*(7), 1471–1490.

Bett, B., & Rice, A. (1992). The influence of hexactinellid sponge (Pheronema carpenteri) spicules on the patchy distribution of macrobenthos in the Porcupine Seabight (Bathyal NE Atlantic). *Ophelia*, *36*(3), 217–226.

Boehlert, G. W., & Genin, A. (1987). A review of the effects of seamounts on biological processes. *Seamounts, Islands, and Atolls*, *43*, 319–334.

Boudreau, B. P., & Jorgensen, B. B. (2001). *The benthic boundary layer: Transport processes and biogeochemistry*. Oxford University Press.

Buhl-Mortensen, L., Vanreusel, A., Gooday, A. J., Levin, L. A., Priede, I. G., Buhl-Mortensen, P., et al. (2010). Biological structures as a source of habitat heterogeneity and biodiversity on the deep ocean margins. *Marine Ecology*, *31*(1), 21–50.

Busch, K., Hanz, U., Mienis, F., Müller, B., Franke, A., Roberts, E. M., et al. (2020). On giant shoulders: How a seamount affects the microbial community composition of seawater and sponges. *Biogeosciences*, *17*:3471–3486.

Cathalot, C., Van Oevelen, D., Cox, T. J., Kutti, T., Lavaleye, M., Duineveld, G., & Meysman, F. J. (2015). Cold-water coral reefs and adjacent sponge grounds: Hotspots of benthic respiration and organic carbon cycling in the deep sea. *Frontiers in Marine Science*, *2*, 37.

Chapman, D. C., & Haidvogel, D. B. (1992). Formation of Taylor caps over a tall isolated seamount in a stratified ocean. *Geophysical & Astrophysical Fluid Dynamics*, *64*(1–4), 31–65.

Chu, J. W., & Leys, S. P. (2010). High resolution mapping of community structure in three glass sponge reefs (Porifera, Hexactinellida). *Marine Ecology Progress Series*, *417*, 97–113.

Clark, M. R., Rowden, A. A., Schlacher, T., Williams, A., Consalvey, M., Stocks, K. I., et al. (2010). The ecology of seamounts: Structure, function, and human impacts. *Annual Review of Marine Science*, *2*, 253–278.

Codiga, D. L. (2011). *Unified tidal analysis and prediction using the UTide Matlab functions*. Graduate School of Oceanography, University of Rhode Island Narragansett.

Coma, R. (2002). Seasonality of in situ respiration rate in three temperate benthic suspension feeders. *Limnology & Oceanography*, *47*(1), 324–331.

Cyr, F., van Haren, H., Mienis, F., Duineveld, G., & Bourgault, D. (2016). On the influence of cold-water coral mound size on flow hydrodynamics, and vice versa. *Geophysical Research Letters*, *43*(2), 775–783.

Conway, K. W., Barrie, J. V., & Krautter, M. (2005). Geomorphology of unique reefs on the western Canadian shelf: Sponge reefs mapped by multibeam bathymetry. *Geo-Marine Letters*, *25*(4), 205–213.

Culwick, T., Phillips, J., Goodwin, C., Rayfield, E. J., & Hendry, K. R. (2020). Sponge density and distribution constrained by fluid forcing in the deep sea. *Frontiers in Marine Science*, *7*, 395.

Davies, A. J., Duineveld, G. C., Lavaleye, M. S., Bergman, M. J., van Haren, H., & Roberts, J. M. (2009). Downwelling and deep-water bottom currents as food supply mechanisms to the cold-water coral Lophelia pertusa (Scleractinia) at the Mingulay Reef Complex. *Limnology & Oceanography*, *54*(2), 620–629.

Davison, J. J., van Haren, H., Hosegood, P., Piechaud, N., & Howell, K. L. (2019). The distribution of deep-sea sponge aggregations (Porifera) in relation to oceanographic processes in the Faroe-Shetland Channel. *Deep Sea Research Part I: Oceanographic Research Papers*, *146*, 55–61.

de Goeij, J. M., van den Berg, H., van Oostveen, M. M., Epping, E. H., & Van Duyl, F. C. (2008). Major bulk dissolved organic carbon (DOC) removal by encrusting coral reef cavity sponges. *Marine Ecology Progress Series*, *357*, 139–151.

Dodds, L., Roberts, J., Taylor, A., & Marubini, F. (2007). Metabolic tolerance of the cold-water coral Lophelia pertusa (Scleractinia) to temperature and dissolved oxygen change. *Journal of Experimental Marine Biology and Ecology*, *349*(2), 205–214.

Duineveld, G. C. A., Lavaleye, M. S. S., & Berghuis, E. M. (2004). Particle flux and food supply to a seamount cold-water coral community (Galicia Bank, NW Spain). *Marine Ecology Progress Series*, *277*, 13–23. https://doi.org/10.3354/meps277013

Duineveld, G. C. A., Lavaleye, M. S. S., Bergman, M. I. N., De Stigter, H., & Mienis, F. (2007). Trophic structure of a cold-water coral mound community (Rockall Bank, NE Atlantic) in relation to the near-bottom particle supply and current regime. *Bulletin of Marine Science*, *81*(3), 449–467.

EMODnet Bathymetry Consortium. (2016). *EMODnet digital bathymetry (DTM)*. EMODnet Bathymetry.

Eriksen, C. C. (1982). Observations of internal wave reflection off sloping bottoms. *Journal of Geophysical Research: Oceans*, *87*(C1), 525–538.

Frederiksen, R., Jensen, A., & Westerberg, H. (1992). The distribution of the scleractinian coral Lophelia pertusa around the Faroe Islands and the relation to internal tidal mixing. *Sarsia*, *77*(2), 157–171.

Freiwald, A. (2002), Reef-forming cold-water corals. In *Ocean margin systems* (pp. 365–385). Springer.

Fugate, D. C., & Friedrichs, C. T. (2002). Determining concentration and fall velocity of estuarine particle populations using ADV, OBS and LISST. *Continental Shelf Research*, *22*(11–13), 1867–1886.

Gooday, A. J. (2002). Biological responses to seasonally varying fluxes of organic matter to the ocean floor: A review. *Journal of Oceanography*, *58*(2), 305–332.

Gostiaux, L., & Van Haren, H. (2010). Extracting meaningful information from uncalibrated backscattered echo intensity data. *Journal of Atmospheric and Oceanic Technology*, *27*(5), 943–949.
Guihen, D., White, M., & Lundälv, T. (2013). Boundary layer flow dynamics at a cold-water coral reef. *Journal of Sea Research*, *78*, 36–44.
Haidvogel, D. B., Beckmann, A., Chapman, D. C., & Lin, R.-Q. (1993). Numerical simulation of flow around a tall isolated seamount. Part II: Resonant generation of trapped waves. *Journal of Physical Oceanography*, *23*(11), 2373–2391.
Hanz, U. (2021a). Long-term monitoring of near-bottom physical properties at an Arctic deep-sea sponge ground. *PANGAEA*. https://doi.org/10.1594/PANGAEA.927956
Hanz, U. (2021b). Physical oceanography during G. O. Sars cruise GS2018108 to an Arctic deep-sea sponge ground in 2018. *PANGAEA*. https://doi.org/10.1594/PANGAEA.927946
Hanz, U. (2021c). Vertical fluxes of organic matter over an annual cycle at an Arctic deep-sea sponge ground. *PANGAEA*. https://doi.org/10.1594/PANGAEA.927955
Hanz, U., & Mienis, F. (2019). *Video: High current event at an Arctic deep-sea sponge ground*. https://doi.org/10.25850/nioz/7b.b.t
Helland-Hansen, B., & Nansen, F. (1909). The Norwegian Sea: its physical oceanography based upon the Norwegian researches 1900-1904. *Det Mallingske bogtrykkeri*.
Henrich, R., Hartmann, M., Reitner, J., Schäfer, P., Freiwald, A., Steinmetz, S., et al. (1992). Facies belts and communities of the Arctic Vesterisbanken Seamount (central Greenland Sea). *Facies*, *27*(1), 71.
Hentschel, U., Usher, K. M., & Taylor, M. W. (2006). Marine sponges as microbial fermenters. *FEMS Microbiology Ecology*, *55*(2), 167–177.
Hochachka, P., & Somero, G. (1968). The adaptation of enzymes to temperature. *Comparative Biochemistry & Physiology*, *27*(3), 659–668.
Hogg, M., Tendal, O., Conway, K., Pomponi, S., Van Soest, R., Gutt, J., et al. (2010). Deep-seas sponge grounds: Reservoirs of biodiversity (Vol. 32). UNEP-WCMC Biodiversity. http://www.unep-wcmc.org/resources/publications/UNEP_WCMC_bio_series/32.aspx
Holm-Hansen, O., Lorenzen, C. J., Holmes, R. W., & Strickland, J. D. (1965). Fluorometric determination of chlorophyll. *ICES Journal of Marine Science*, *30*(1), 3–15.
Hopkins, T. S. (1991). The GIN Sea—A synthesis of its physical oceanography and literature review 1972–1985. *Earth-Science Reviews*, *30*(3–4), 175–318.
Hosegood, P., Nimmo-Smith, W., Proud, R., Adams, K., & Brierley, A. (2019). Internal lee waves and baroclinic bores over a tropical seamount shark "hot-spot". *Progress in Oceanography*, *172*, 34–50.
Howell, K. L., Piechaud, N., Downie, A. L., & Kenny, A. (2016). The distribution of deep-sea sponge aggregations in the North Atlantic and implications for their effective spatial management. *Deep Sea Research Part I: Oceanographic Research Papers*, *115*, 309–320.
Huthnance, J. M. (1989). Internal tides and waves near the continental shelf edge. *Geophysical & Astrophysical Fluid Dynamics*, *48*(1-3), 81–106.
Jakobsson, M., Mayer, L., Coakley, B., Dowdeswell, J. A., Forbes, S., Fridman, B., et al. (2012). The international bathymetric chart of the Arctic Ocean (IBCAO) version 3.0. *Geophysical Research Letters*, *39*(12).
Jalali, M., VanDine, A., Chalamalla, V. K., & Sarkar, S. (2017). Oscillatory stratified flow over supercritical topography: Wave energetics and turbulence. *Computers & Fluids*, *158*, 39–48.
Jeansson, E., Olsen, A., & Jutterström, S. (2017). Arctic intermediate water in the Nordic Seas, 1991–2009. *Deep Sea Research Part I: Oceanographic Research Papers*, *128*, 82–97.
Kahn, A. S., Chu, J. W., & Leys, S. P. (2018). Trophic ecology of glass sponge reefs in the Strait of Georgia, British Columbia. *Scientific Reports*, *8*(1), 756. https://doi.org/10.1038/s41598-017-19107-x
Kahn, A. S., Yahel, G., Chu, J. W., Tunnicliffe, V., & Leys, S. P. (2015). Benthic grazing and carbon sequestration by deep-water glass sponge reefs. *Limnology & Oceanography*, *60*(1), 78–88. https://doi.org/10.1002/lno.10002
King, J. R., & Farner, D. S. (1961). Energy metabolism, thermoregulation and body temperature. *Biology and comparative physiology of birds*, *2*, 215–288.
Kiriakoulakis, K., Stutt, E., Rowland, S. J., Vangriesheim, A., Lampitt, R. S., & Wolff, G. A. (2001). Controls on the organic chemical composition of settling particles in the Northeast Atlantic Ocean. *Progress in Oceanography*, *50*(1–4), 65–87.
Klitgaard, A. B., & Tendal, O. S. (2004). Distribution and species composition of mass occurrences of large-sized sponges in the northeast Atlantic. *Progress in Oceanography*, *61*(1), 57–98.
Knies, J., & Martinez, P. (2009). Organic matter sedimentation in the western Barents Sea region: Terrestrial and marine contribution based on isotopic composition and organic nitrogen content. *Norwegian Journal of Geology/Norsk Geologisk Forening*, *89*, 79–89.
Lampitt, R., & Antia, A. (1997). Particle flux in deep seas: Regional characteristics and temporal variability. *Deep Sea Research Part I: Oceanographic Research Papers*, *44*(8), 1377–1403.
Lavelle, J. W., & Mohn, C. (2010). Motion, commotion, and biophysical connections at deep ocean seamounts. *Oceanography*, *23*(1), 90–103.
Maldonado, M., Aguilar, R., Bannister, R. J., Bell, J. J., Conway, K. W., Dayton, P. K., et al. (2017). Sponge grounds as key marine habitats: A synthetic review of types, structure, functional roles, and conservation concerns. *Marine Animal Forests: The Ecology of Benthic Biodiversity Hotspots*, 145–183. https://doi.org/10.1007/978-3-319-21012-4_24
Maldonado, M., Aguilar, R., Blanco, J., García, S., Serrano, A., & Punzón, A. (2015). Aggregated clumps of Lithistid sponges: A singular, reef-like bathyal habitat with relevant paleontological connections. *PloS One*, *10*(5), e0125378.
Meyer, H., Roberts, E., Rapp, H., & Davies, A. (2019). Spatial patterns of arctic sponge ground fauna and demersal fish are detectable in autonomous underwater vehicle (AUV) imagery. *Deep Sea Research Part I: Oceanographic Research Papers*, *153*, 103137. https://doi.org/10.1016/j.dsr.2019.103137
Mienis, F., Bouma, T., Witbaard, R., van Oevelen, D., & Duineveld, G. (2019). Experimental assessment of the effects of coldwater coral patches on water flow. *Marine Ecology Progress Series*, *609*, 101–117.
Mienis, F., Duineveld, G., Davies, A., Ross, S., Seim, H., Bane, J., & Van Weering, T. (2012). The influence of near-bed hydrodynamic conditions on cold-water corals in the Viosca Knoll area, Gulf of Mexico, *Deep Sea Research Part I: Oceanographic Research Papers*, *60*, 32–45.
Mourino, B., Fernández, E., Serret, P., Harbour, D., Sinha, B., & Pingree, R. (2001). Variability and seasonality of physical and biological fields at the Great Meteor Tablemount (subtropical NE Atlantic). *Oceanologica Acta*, *24*(2), 167–185.
Müller, P., & Liu, X. (2000). Scattering of internal waves at finite topography in two dimensions. Part I: Theory and case studies. *Journal of physical oceanography*, *30*(3), 532–549.
Murillo, F. J., Muñoz, P. D., Cristobo, J., Ríos, P., González, C., Kenchington, E., & Serrano, A. (2012). Deep-sea sponge grounds of the Flemish Cap, Flemish Pass and the Grand Banks of Newfoundland (Northwest Atlantic Ocean): Distribution and species composition. *Marine Biology Research*, *8*(9), 842–854.
Munk, W. H. (1980). Internal wave spectra at the buoyant and inertial frequencies. *Journal of Physical Oceanography*, *10*(11), 1718–1728.

Nöthig, E.-M., & von Bodungen, B. (1989). Occurrence and vertical flux of faecal pellets of probably protozoan origin in the southeastern Weddell Sea (Antarctica). *Marine Ecology Progress Series*, *56*, 281–289.

Oevelen, D. v., Duineveld, G., Lavaleye, M., Mienis, F., Soetaert, K., & Heip, C. H. (2009). The cold-water coral community as hotspot of carbon cycling on continental margins: A food-web analysis from Rockall Bank (northeast Atlantic). *Limnology & Oceanography*, *54*(6), 1829–1844.

Radax, R., Hoffmann, F., Rapp, H. T., Leininger, S., & Schleper, C. (2012). Ammonia-oxidizing archaea as main drivers of nitrification in cold-water sponges. *Environmental Microbiology*, *14*(4), 909–923.

Radax, R., Rattei, T., Lanzen, A., Bayer, C., Rapp, H. T., Urich, T., & Schleper, C. (2012). Metatranscriptomics of the marine sponge *Geodia barretti*: Tackling phylogeny and function of its microbial community. *Environmental Microbiology*, *14*(5), 1308–1324. https://doi.org/10.1111/j.1462-2920.2012.02714.x

Reiswig, H. M. (1975). Bacteria as food for temperate-water marine sponges. *Canadian Journal of Zoology*, *53*(5), 582–589.

Rice, A., Thurston, M., & New, A. (1990). Dense aggregations of a hexactinellid sponge, Pheronema carpenteri, in the Porcupine Seabight (northeast Atlantic Ocean), and possible causes. *Progress in Oceanography*, *24*(1–4), 179–196.

Rix, L., de Goeij, J. M., van Oevelen, D., Struck, U., Al-Horani, F. A., Wild, C., & Naumann, M. S. (2017). Differential recycling of coral and algal dissolved organic matter via the sponge loop. *Functional Ecology*, *31*(3), 778–789.

Roberts, E., Mienis, F., Rapp, H., Hanz, U., Meyer, H., & Davies, A. (2018). Oceanographic setting and short-timescale environmental variability at an Arctic seamount sponge ground. *Deep Sea Research Part I: Oceanographic Research Papers*, *138*, 98–113. https://doi.org/10.1016/j.dsr.2018.06.007

Robertson, R., Dong, J., & Hartlipp, P. (2017). Diurnal Critical latitude and the latitude dependence of internal tides, internal waves, and mixing based on Barcoo seamount. *Journal of Geophysical Research: Oceans*, *122*(10), 7838–7866.

Rudels, B., Fahrbach, E., Meincke, J., Budéus, G., & Eriksson, P. (2002). The East Greenland Current and its contribution to the Denmark Strait overflow. *ICES Journal of Marine Science*, *59*(6), 1133–1154.

Rudnick, D. L., Boyd, T. J., Brainard, R. E., Carter, G. S., Egbert, G. D., Gregg, M. C., et al. (2003). From tides to mixing along the Hawaiian Ridge. *Science*, *301*(5631), 355–357.

Schlitzer, R. (2015). Ocean data view, edited.

Smetacek, V. (1984), The supply of food to the benthos. In *Flows of energy and materials in marine ecosystems*, edited, pp. 517–547. Springer.

Somero, G. (1998). Adaptation to cold and depth: Contrasts between polar and deep-sea animals. *Cold ocean physiology*, *66*, 33–57.

Strand, R., Whalan, S., Webster, N. S., Kutti, T., Fang, J. K.-H., Luter, H. M., & Bannister, R. (2017). The response of a boreal deep-sea sponge holobiont to acute thermal stress. *Scientific Reports*, *7*(1), 1660.

Sverdrup, H. (1953). On conditions for the vernal blooming of phytoplankton. *ICES Journal of Marine Science*, *18*(3), 287–295.

Tabachnick, K., Van Soest, R., van Kempen Th, M., & Braekamn, J. (1994). *Distribution of recent Hexactinellida, sponges in time and space*. Balkema.

Taylor, G. I. (1923). Experiments on the motion of solid bodies in rotating fluids. *Proceedings of the Royal Society of London. Series A*, *104*(725), 213–218.

Taylor, J. R. (1993). Turbulence and mixing in the boundary layer generated by shoaling internal waves. *Dynamics of Atmospheres and Oceans*, *19*(1–4), 233–258.

Vacelet, J., & Boury-Esnault, N. (1995). Carnivorous sponges. *Nature*, *373*(6512), 333–335.

van Haren, H., & Gostiaux, L. (2012). Detailed internal wave mixing above a deep-ocean slope. *Journal of Marine Research*, *70*(1), 173–197.

van Haren, H., Hanz, U., de Stigter, H., Mienis, F., & Duineveld, G. (2017). Internal wave turbulence at a biologically rich Mid-Atlantic seamount. *PloS One*, *12*(12), e0189720.

van Haren, H., Mienis, F., Duineveld, G. C., & Lavaleye, M. S. (2014). High-resolution temperature observations of a trapped nonlinear diurnal tide influencing cold-water corals on the Logachev mounds. *Progress in Oceanography*, *125*, 16–25.

Vilas, J., Arístegui, J., Kiriakoulakis, K., Wolff, G., Espino, M., Polo, I., et al. (2009). Seamounts and organic matter—Is there an effect? The case of Sedlo and Seine Seamounts: Part 1. Distributions of dissolved and particulate organic matter. *Deep Sea Research Part II: Topical Studies in Oceanography*, *56*(25), 2618–2630.

Wakeham, S. G., Hedges, J. I., Lee, C., & Pease, T. K. (1993). Effects of poisons and preservatives on the composition of organic matter in a sediment trap experiment. *Journal of Marine Research*, *51*(3), 669–696.

Wassmann, P., Peinert, R., & Smetacek, V. (1991). Patterns of production and sedimentation in the boreal and polar Northeast Atlantic. *Polar Research*, *10*(1), 209–228.

Witte, U., Brattegard, T., Graf, G., & Springer, B. (1997). Particle capture and deposition by deep-sea sponges from the Norwegian-Greenland Sea. *Marine Ecology Progress Series*, *154*, 241–252.

Yahel, G., Eerkes-Medrano, D. I., & Leys, S. P. (2006). Size independent selective filtration of ultraplankton by hexactinellid glass sponges. *Aquatic Microbial Ecology*, *45*(2), 181–194.

Yang, T.-H., & Somero, G. N. (1993). Effects of feeding and food deprivation on oxygen consumption, muscle protein concentration and activities of energy metabolism enzymes in muscle and brain of shallow-living (Scorpaena guttata) and deep-living (Sebastolobus Alaskan's) scorpaenid fishes. *Journal of Experimental Biology*, *181*(1), 213–232.